This is the peer reviewd version of the followng article:

SURFACE ELASTICITY EFFECTS IN PIN-HOLE CONTACT WITH RADIAL CLEARANCE / Radi, E.. - In: EUROPEAN JOURNAL OF MECHANICS. A, SOLIDS. - ISSN 0997-7538. - (2026), pp. 1-11. [10.1016/j.euromechsol.2026.106294]

Terms of use:

The terms and conditions for the reuse of this version of the manuscript are specified in the publishing policy. For all terms of use and more information see the publisher's website.

22/07/2026 11:35

(Article begins on next page)

European Journal of Mechanics / A Solids xxx (xxxx) 106294

Contents lists available at ScienceDirect

European Journal of Mechanics / A Solids

journal homepage: www.elsevier.com/locate/ejmsol

ELSEVIER

Full Length Article

Surface elasticity effects in pin-hole contact with radial clearance

E. Radi[a,b]

[a] DISMI - Dipartimento di Scienze e Metodi dell'Ingegneria, Università di Modena e Reggio Emilia, Via G. Amendola 2, Reggio Emilia, I-42122, Italy
[b] En&Tech - Centro di Ricerca Interdipartimentale per la Ricerca Industriale ed il Trasferimento Tecnologico, Reggio Emilia, 42122, Italy

ARTICLE INFO

Keywords:
Pinned joint
Surface elasticity
Dual series equations
Advancing contact
Clearance

ABSTRACT

This work investigates the frictionless contact of a loaded rigid circular pin inserted with radial clearance into a circular hole in an infinite isotropic elastic plane, with the hole boundary described by surface elasticity theory. The problem is motivated by small-scale mechanical systems and by surface-treated pin joints, where the near-surface region may have mechanical properties that differ from those of the bulk material. The elastic field in the plane is represented by the Michell solution in cylindrical coordinates, while the hole boundary is endowed with surface elastic properties according to the Gurtin–Murdoch model. The resulting surface stress modifies the classical traction boundary conditions through curvature-dependent and surface-gradient terms. By imposing the unilateral frictionless contact conditions, the problem is reduced to a system of dual trigonometric series equations, which are transformed into an infinite system of linear algebraic equations and solved numerically by truncation. The analysis focuses on the influence of surface elasticity on the contact semi-angle, contact pressure distribution, and hoop stress at the hole rim. Comparisons with the classical solution show how surface elastic parameters can modify the contact pressure transmitted through the pin–hole interface and smooth the hoop stress concentration around the hole. The results are then supported by verifying that the M-integral remains invariant along arbitrary circular contours enclosing the hole. The formulation provides an extension of classical pin-loaded hole theory to cases where surface effects, surface treatments, or small geometric length scales are mechanically significant.

UNCORRECTED PROOF

1. Introduction

Contact between a rigid pin and an elastic plate containing a circular hole is a classical problem in contact mechanics, with direct relevance to pin-jointed structural components, mechanical fasteners, bushings, bearings, composite joints, and micro- and nano-mechanical devices (Rao et al., 1977; Rao, 1978; Ho and Chau, 1997; Mizushima and Hamada, 1983; Ciavarella and Decuzzi, 2001a, 2001b,b; Hou and Hills, 2001; Iyer, 2001; Yavari et al., 2008; Nguyen-Hoang and Becker, 2021, 2021b; Nguyen and Nguyen, 2025a,b; Radi and Güler, 2026a, 2026b). In its conventional formulation, a rigid circular inclusion or pin is inserted into a circular hole of an infinite elastic plane, with a prescribed radial clearance and an external load applied to the pin. In real joints, clearance is necessarily introduced because it allows the connected bodies to move relative to each other. As a consequence, the load is transmitted to the surrounding elastic medium through a finite contact arc along the hole boundary, whose length increases with the load magnitude. Determining the resulting distribution of contact pressure and hoop stress at the hole rim is essential for predicting local failure, crack initiation, fretting damage, and stress concentration effects.

For macroscopic systems, the hole boundary is usually treated as a classical traction boundary, and the material response is described by bulk elasticity only. Under this assumption, the contact pressure and rim stresses are governed by the pin-hole clearance, the applied load, the relative stiffness of the contacting bodies, and the extent of the contact zone. For frictionless contact, the tangential tractions vanish and only normal compressive tractions are transmitted across the interface. Although this idealization has enabled analytical and semi-analytical treatments of the pin-loaded hole problem, it neglects effects associated with the energetic and mechanical response of the surface itself. Such surface effects become increasingly important when the characteristic length scale of the problem decreases, for example in micro- and nano-electromechanical systems, thin coatings, small-scale connectors, porous materials with nanoscale voids, and architected materials containing small holes or inclusions. At these scales, the surface-to-volume ratio is large, and the mechanical behavior of a free or contacted boundary may differ significantly from that predicted by classical elasticity. Surface elasticity theory, commonly formulated through the Gurtin-Murdoch surface elasticity theory (Gurtin and Murdoch, 1975, 1978)

E-mail addresses: enrico.radi@unimore.it, eradi@unimore.it (E. Radi).

https://doi.org/10.1016/j.euromechsol.2026.106294
Received 1 June 2026; Received in revised form 12 July 2026; Accepted 16 July 2026
0997-7538/© 20XX

provides a continuum framework for incorporating these effects. In this approach, the boundary is endowed with its own elastic properties, including residual surface tension and surface elastic moduli. As a result, the boundary conditions at the hole rim are modified, and the stress field in the surrounding bulk material becomes size-dependent.

The Gurtin–Murdoch model has been extensively adopted in the literature when considering contact problems at the nanoscale. For example, Wang and Feng (2007) used the Fourier integral transform method to derive the general solution for the contact problem under pressure. Long et al. (2012) numerically investigated the contact problem of a rigid cylinder indenting on an elastic half space with surface tension. Zhou and Gao (2013) provided analytical and numerical solutions for the problems of an elastic half-space and an elastic half-plane with surface elasticity subjected to a distributed normal force or indented by spherical or conical punches. Li and Mi (2019), Zemlyanova and White (2022) studied the contact problem between a rigid sphere or a more general axisymmetric stamp and an elastic half-plane with surface elasticity. All these investigations revealed that the presence of surface tension decreases the magnitude of the displacement field and yields a more uniform distribution of the normal pressure in the contact region compared to the classical elasticity-based solutions. Consequently, for contact problems at the nanoscale, surface elasticity significantly affects the interaction between contacting bodies, altering key quantities such as contact stress distribution, contact stiffness and strength. Its inclusion is therefore essential for accurately describing and predicting nanoscale contact behavior. Indeed, atomistic simulations and experimental testing suggested that surface effects play a critical role in nanosized contact problems (Horstemeyer and Baskes, 1999; Gerberich et al., 2002).

Beyond size-dependent effects in micro- and nano-scale solids, surface elasticity is also relevant to the modelling of mechanically treated pin joints. In many load-transfer components, the contact surface is deliberately modified by carburizing, nitriding, induction hardening, or related surface-treatment techniques in order to generate a hard surface layer while retaining a comparatively deformable core (Mencik, 2013; Osborn, 1941). This combination improves component performance by increasing wear resistance and durability under high contact loads, reducing frictional degradation in practical applications, and hindering crack initiation and crack growth under cyclic loading (Persson et al., 1997). Chau and Wei (2001) analytically investigated stress mitigation around a loaded circular inclusion achieved by embedding a reinforced ring around a hole in an infinite elastic plane. They derived closed-form expressions for the stresses induced in an inclusion, or rivet, perfectly bonded to the elastic plane through the reinforced ring. They showed that the tensile hoop stress can be reduced to a negligible level by assigning an appropriate stiffness to the reinforced ring, provided that the ring is stiffer than the surrounding plane. Consequently, the near-surface mechanical response may play a decisive role in determining the pressure transmitted through the pin–hole interface and the stress concentration developed around the hole boundary. When the thickness of the treated layer is small relative to the hole radius, surface elasticity theory offers a convenient reduced-order description of its mechanical influence, replacing an explicitly layered model by an effective elastic boundary. In this sense, the present formulation is relevant not only to small-scale contact problems, but also to engineered pin joints in which surface treatments are used to enhance wear resistance, fatigue strength, and service life.

The inclusion of surface elasticity is also highly relevant in biomechanics, particularly for the mechanical modeling of bone structures. Indeed, many biological tissues, and cortical bone in particular, exhibit a heterogeneous architecture characterized by a relatively stiff outer layer surrounding a softer and more porous inner bulk region. In this context, surface elasticity provides an effective continuum framework for capturing the mechanical contribution of the stiff cortical layer and its interaction with the underlying trabecular structure.

Despite extensive studies of circular holes, rigid inclusions, and pin-loaded elastic plates within classical elasticity, comparatively little attention has been paid to the role of surface elasticity in pin-hole contact problems with clearance. This gap is significant because the contact pressure distribution is highly sensitive to the local boundary compliance, while the hoop stress at the hole rim is one of the key quantities controlling damage initiation. Surface elasticity can alter both the magnitude and distribution of these fields, potentially changing the predicted contact-zone size, peak contact pressure, and stress concentrations around the hole. Therefore, classical solutions may become inadequate when the hole radius is comparable to the intrinsic length scales associated with surface elastic properties.

Although there is a consistent amount of research on modeling the clearance and investigating its influence on the contact response of pinned joints, very limited attention has been devoted to qualitative analysis of the effect of surface elasticity in clearance joints on the contact response.

The present study addresses these issues by analyzing the frictionless contact of a loaded rigid circular pin inserted with clearance into a circular hole in an infinite elastic plane, where the hole rim is modeled using surface elasticity theory. The main novelty of the work lies in explicitly incorporating the elastic response of the hole boundary into the pin-hole contact formulation and investigating its influence on two mechanically critical quantities: the contact pressure acting over the pin-hole interface and the hoop stress along the hole rim. By comparing the surface-elastic solution with the corresponding classical prediction, the present study clarifies how surface parameters modify the contact response and identifies the regimes in which surface effects become non-negligible.

Particular emphasis is placed on the redistribution of contact pressure and hoop stress caused by the surface-elastic boundary. Since the surface layer contributes additional stiffness (Altenbach et al., 2011) and introduces curvature-dependent stress terms, it may amplify or reduce the local contact pressure depending on the surface material constants, hole size, clearance, and applied load. This redistribution influences the location and magnitude of the peak equivalent stress, which are central to assessing local yielding, wear, and interfacial damage. The analysis of the corresponding stress variations provides insight into the mechanical role of surface elasticity in pin-loaded holes and in related small-scale or surface-treated contact systems.

The remainder of the paper is organized as follows. In Section 2, the stress and displacement fields in the elastic plane are expressed in cylindrical coordinates through the Michell solution for isotropic linear elasticity (Barber, 2010). The frictionless unilateral contact conditions are then imposed together with the modified boundary conditions induced by surface elasticity at the hole rim. This formulation reduces the pin–hole contact problem with clearance to a set of dual trigonometric series equations, in which the surface elastic parameters enter explicitly through the boundary conditions. In Section 3, following the approach developed by Radi and Strozzi (2023) the dual series equations are converted into an infinite system of linear algebraic equations for the unknown coefficients of the stress and displacement fields. This system is subsequently solved by truncation. Section 4 presents and discusses the results obtained for the contact angle, contact pressure distribution, hoop stress at the hole boundary, and displacement fields for different loading levels, clearances, and surface elastic properties. The paper then discusses the implications of surface elasticity for the extension of classical pin-hole contact theory to problems in which boundary effects cannot be neglected. The results obtained in this study suggest that the presence of a stiff surface layer can substantially modify the contact pressure distribution, stress transfer mechanisms, and effective contact area, all of which are key factors in the analysis of load transmission, wear, and damage evolution also in biological joints.

The limiting cases recover the corresponding classical elasticity results when the surface elastic parameters are set to zero. An additional consistency check of the obtained results is then provided in Section 5 based on the invariance property of the M-integral.

In addition to contributing to the fundamental understanding of contact mechanics with surface elasticity, the study may be useful for the

UNCORRECTED PROOF

design and reliability assessment of miniaturized mechanical joints, microstructured elastic solids, coated or functionalized holes, and materials containing nanoscale perforations. It may also serve as an idealized two-dimensional model for biomechanical applications involving joint contact mechanics, such as the interaction between the artificial femoral head and the acetabular cavity in the hip joint.

2. Governing equations and contact conditions

Reference is made to a cylindrical coordinate system (r, θ, z) centered at the circular hole in the elastic plane, with $\theta = 0$ aligned with the direction of the applied pin force (Fig. 1). Let the elastic matrix occupy the region $r > R$, where R is the radius of the hole. A rigid circular pin of radius a, with $a < R$, is inserted with clearance, $\delta = R - a$, in the hole. The bulk material is assumed to be isotropic, linear elastic, and governed by plane strain or plane stress elasticity. Its material response is thus characterized by the shear modulus μ and Poisson's ratio ν. The load P applied to the pin produces contact over an angular region of extent 2α, which increases with increasing load because of the presence of radial clearance.

The general expressions of the stress and displacement fields in the elastic region follows from the classical Michell solution (Barber, 2010), where only the stress terms vanishing at infinity and yielding single valued displacement are retained, namely

$$\frac{\sigma_{rr}R}{2\mu\delta} = D_0\left(\frac{R}{r}\right)^2 + \left[D_1(2-\rho^2)\frac{R}{r} - 2C_1\left(\frac{R}{r}\right)^3\right]\cos\theta$$
$$-\sum_{n=2}^{\infty}\left[C_n\, n\,(n+1)\left(\frac{R}{r}\right)^{n+2} + D_n\,(n+2)(n-1)\left(\frac{R}{r}\right)^n\right]\cos n\theta,$$
$$\frac{\sigma_{\theta\theta}R}{2\mu\delta} = -D_0\left(\frac{R}{r}\right)^2 - \left[D_1\,\rho^2\frac{R}{r} - 2C_1\left(\frac{R}{r}\right)^3\right]\cos\theta$$
$$+\sum_{n=2}^{\infty}\left[C_n\, n\,(n+1)\left(\frac{R}{r}\right)^{n+2} + D_n\,(n-2)(n-1)\left(\frac{R}{r}\right)^n\right]\cos n\theta,$$
$$\frac{\sigma_{r\theta}R}{2\mu\delta} = -\left[D_1\,\rho^2\frac{R}{r} + 2C_1\left(\frac{R}{r}\right)^3\right]\sin\theta$$
$$-\sum_{n=2}^{\infty}\left[\mathrm{C_n}\,(\mathrm{n}+1)\left(\frac{\mathrm{R}}{\mathrm{r}}\right)^{\mathrm{n}+2}\right.$$
$$\left.+\mathrm{D_n}\,(\mathrm{n}-1)\left(\frac{\mathrm{R}}{\mathrm{r}}\right)^{\mathrm{n}}\right]\mathrm{n}\;\;\mathrm{sinn}\,\theta, \tag{2.1}$$
$$\frac{u_r}{\delta} = -D_0\frac{R}{r} + \left\{C_1\left(\frac{R}{r}\right)^2 - D_1\left[(1+\rho^2)\ln\frac{R}{r} + \frac{1-\rho^2}{2}\right]\right\}\cos\theta$$
$$+\sum_{n=2}^{\infty}\left[C_n\, n\left(\frac{R}{r}\right)^{n+1} + D_n\left(\frac{2\rho^2}{1-\rho^2}+n\right)\left(\frac{R}{r}\right)^{n-1}\right]\cos n\theta,$$
$$\frac{u_\theta}{\delta} = \left\{C_1\left(\frac{R}{r}\right)^2 + D_1\left[(1+\rho^2)\ln\frac{R}{r} - \frac{1-\rho^2}{2}\right]\right\}\sin\theta$$
$$+\sum_{n=2}^{\infty}\left[C_n\, n\left(\frac{R}{r}\right)^{n+1} - D_n\left(\frac{2}{1-\rho^2}-n\right)\left(\frac{R}{r}\right)^{n-1}\right]\sin n\theta.$$

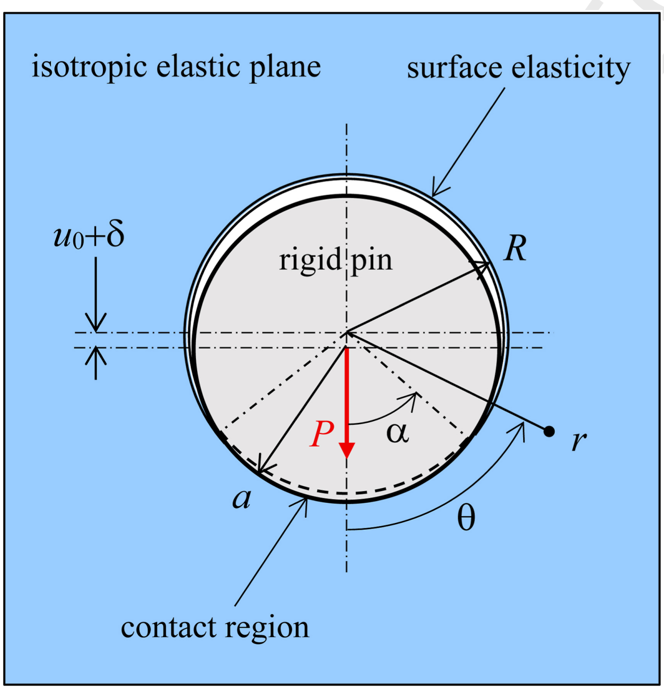

Fig. 1. Rigid pin of radius a loaded by a line force P and fitted with clearance into a hole in an infinite elastic plane with surface elasticity. The pin-hole interaction occurs over a contact arc of angular extent 2α. The pin displacement is denoted by u_0, and δ is the radial clearance. A cylindrical reference coordinate system is introduced centered at the hole centre with the angular coordinate $\theta = 0$ aligned with the direction of the applied pin force.

The unknown coefficients D_0, C_i, and D_i ($i = 1, 2, \ldots$) in Eq. (2.1) can be determined from the boundary conditions at $r = R$. Moreover, the following constitutive parameter is introduced

$$\rho^2 = \frac{1-2\bar{\nu}}{2(1-\bar{\nu})}, \qquad \text{where} \quad \bar{\nu} = \begin{cases} \nu & \text{for plane strain,} \\ \dfrac{\nu}{1+\nu} & \text{for plane stress.} \end{cases} \tag{2.2}$$

At the hole boundary, the surface is modeled as an elastic membrane following the Gurtin–Murdoch surface elasticity theory. The surface strain ε_s and the surface tensile load τ are defined as [7]

$$\varepsilon_s = \frac{1}{R}(u_{\theta,\theta} + u_r)_{r=R}, \qquad \tau = S_0\,\varepsilon_s, \tag{2.3}$$

respectively, where S_0 is the surface elastic modulus. For a circular boundary loaded by a distributed pressure $p(\theta)$, the modified boundary conditions at $r = R$ can be written as

$$\sigma_{rr} - \frac{S_0}{R}\varepsilon_s = -p(\theta), \tag{2.4}$$

$$\sigma_{r\theta} + \frac{S_0}{R}\varepsilon_{s,\theta} = 0. \tag{2.5}$$

with respect to the complete Gurtin-Murdoch model, here the residual surface tension has been deliberately neglected in order to isolate the effect of the strain-dependent part of the Gurtin–Murdoch surface stress. This assumption covers those cases in which the residual surface tension is small as compared to the elastic properties of the material surface. Moreover, a residual surface stress would induce an additional hydrostatic-pressure-type loading. In particular, for a curved boundary/interface, a constant surface tension produces a normal traction proportional to the local curvature, in analogy with the Young–Laplace pressure. Therefore, its inclusion would generally modify the boundary conditions through an additional curvature-dependent normal stress.

Using Eqn. (2.2)-(2.5), the frictionless contact conditions between the rigid pin and the inner rim of the hole in the elastic plane require at $r = R$ (Mogilevskaya et al., 2019):

$$\begin{aligned}
&\sigma_{r\theta} + \frac{S_0}{R^2}\left(u_{\theta,\theta\theta} + u_{r,\theta}\right) = 0, \qquad \text{for} \quad 0 \le |\theta| \le \pi,\\
&\sigma_{rr} - \frac{S_0}{R^2}\left(u_{\theta,\theta} + u_r\right) = 0, \qquad \text{for} \quad \alpha \le |\theta| \le \pi, \qquad (2.6)\\
&u_r = v_0 \ \cos\theta - \delta\,(1-\cos\theta), \qquad \text{for} \quad 0 \le |\theta| \le \alpha,
\end{aligned}$$

where v_0 denotes a rigid body motion of the pin along the loading direction. The contact condition $(2.6)_3$ holds for small clearance $\delta \ll R$, as discussed by Liu et al. (2007), Persson (1964), Ciavarella and Decuzzi (2001a,b), and Hou and Hills (2001).

Usually, surface stresses have a regularizing effect on the mechanical fields. Indeed, the surface elasticity introduces additional tangential differential terms in the boundary conditions (2.6). As a result, the boundary response is no longer governed only by the classical local traction-displacement relation, but also by derivatives of the displacement along the surface. These higher-order surface contributions penalize rapid spatial variations of the displacement field along the boundary and therefore tend to smooth the displacement and stress fields near the surface/interface. In particular, singular or strongly localized variations predicted by the classical solution are expected to be weakened when the surface elastic moduli are nonzero.

3. Reduction to a linear system of algebraic equations

The introduction of the stress and displacement fields (2.1) in the boundary conditions $(2.6)_1$, then yields the following relations for the unknown coefficients C_i ($i = 1, 2, \ldots$) that appear in Eq. (2.1):

$$\begin{aligned}
&C_1 = \frac{(1-\rho^2)\,\lambda - \rho^2}{2(1+\lambda)} D_1,\\
&C_n = -\frac{n-1}{(n+1)(1+n\lambda)}\left(1 + n\lambda - \frac{2\lambda\rho^2}{1-\rho^2}\right) D_n, \qquad (n = 2, 3, \ldots)
\end{aligned} \qquad (3.1)$$

where

$$\lambda = \frac{S_0}{2\mu\, R}, \qquad (3.2)$$

denotes the normalized surface elastic modulus. The introduction of Eq. (3.1) in the stress and displacement fields (2.1) evaluated at the hole rim, namely at $r = R$, then yields,

$$\begin{aligned}
\frac{\sigma_{rr} R}{2\mu\delta} &= D_0 + \frac{2+\lambda}{1-\lambda} D_1 \ \cos\theta - 2\sum_{n=2}^{\infty} \frac{n-1}{1+n\lambda}\left(1 + \frac{n\lambda}{1-\rho^2}\right) D_n \ \cos n\theta,\\
\frac{\sigma_{\theta\theta} R}{2\mu\delta} &= -D_0 + \left(\frac{\lambda}{1-\lambda} - 2\rho^2\right) D_1 \ \cos\theta - 2\sum_{n=2}^{\infty} \frac{n-1}{1+n\lambda}\left(1 + \frac{1-2\rho^2}{1-\rho^2} n\lambda\right) D_n \ \cos n\theta,\\
\frac{\sigma_{r\theta} R}{2\mu\delta} &= -\frac{\lambda}{1-\lambda} D_1 \ \sin\theta - \frac{2\rho^2}{1-\rho^2} \sum_{n=2}^{\infty} \frac{n-1}{1+n\lambda} n\lambda\, D_n \ \sin n\theta, \qquad (3.3)\\
\frac{u_r}{\delta} &= -D_0 - \frac{D_1 \ \cos\theta}{2(1+\lambda)} + \frac{2}{1-\rho^2}\sum_{n=2}^{\infty} \frac{n + \rho^2 + (1+\rho^2) n^2 \lambda}{(n+1)(1+n\lambda)} D_n \cos n\theta,\\
\frac{u_\theta}{\delta} &= -\frac{D_1 \ \sin\theta}{2(1+\lambda)} - \frac{2}{1-\rho^2}\sum_{n=2}^{\infty} \frac{1 + n\lambda + (1+\lambda) n\, \rho^2}{(n+1)(1+n\lambda)} D_n \sin n\theta.
\end{aligned}$$

Using Eq. (3.3), the contact conditions $(2.6)_{2,3}$ then yield the following dual series equations

$$\frac{1+\lambda}{2} D_0 + D_1 \ \cos\theta - \sum_{n=2}^{\infty} D_n \frac{n-1}{\lambda n + 1}\left(1 + \frac{n-\rho^2}{1-\rho^2}\lambda\right) \cos n\theta = 0, \qquad \text{for} \ \ \alpha \le |\theta| \le \pi, \qquad (3.4)$$

$$D_0 - 1 + \left[\frac{D_1}{2(1+\lambda)} + 1 + \frac{v_0}{\delta}\right] \cos\theta - 2\sum_{n=2}^{\infty} D_n \frac{n + \rho^2 + \lambda n^2 (1+\rho^2)}{(n+1)(1+\lambda n)(1-\rho^2)} \cos n\theta = 0, \qquad \text{for} \ \ 0 \le |\theta| \le \alpha. \qquad (3.5)$$

Eqs. (3.4) and (3.5) can be rewritten in the form

$$\frac{A_0}{2} + \sum_{n=1}^{\infty} A_n \ \cos n\theta = 0, \qquad \text{for} \quad \alpha \le |\theta| \le \pi, \qquad (3.6)$$

$$\frac{1}{2(1+\rho^2)}\left(\frac{A_0}{1+\lambda} - 1\right) + \left(\frac{A_1}{2+2\lambda} + \frac{v_0}{\delta} + 1\right)\frac{\cos\theta}{2(1+\rho^2)} + \sum_{n=2}^{\infty} A_n f_n \ \cos n\theta = 0, \ \text{for} \ \ 0 \le |\theta| \le \alpha, \qquad (3.7)$$

where

$$\begin{aligned}
&A_0 = D_0(1+\lambda),\\
&A_1 = D_1, \qquad (3.8)\\
&A_n = -(n-1)\frac{1 - \rho^2 + \lambda n - \lambda\rho^2}{(1-\rho^2)(1+\lambda n)} D_n, \qquad (n = 2, 3, \ldots).
\end{aligned}$$

and

$$f_n = \frac{n + \rho^2 + \lambda n^2 (1+\rho^2)}{(n^2-1)(1-\rho^2+\lambda n - \lambda\rho^2)(1+\rho^2)}, \ (\text{for } n = 2, 3, \ldots). \qquad (3.9)$$

The limiting behavior of f_n as $n \to \infty$ depends on the value of λ. Indeed, if $\lambda > 0$ then

$$f_n = \frac{1}{n} + O(n^{-2}), \qquad \text{as} \quad n \to \infty, \qquad (3.10)$$

whereas for $\lambda = 0$ one has

$$f_n = \frac{1}{n(1-\rho^4)} + O(n^{-2}), \qquad \text{as} \quad n \to \infty. \qquad (3.11)$$

The operator

$$L[\phi] = \frac{d\phi}{d\theta} + \int_0^\theta \phi(s) \ ds, \qquad (3.12)$$

is then applied on equation (3.7) to remove the rigid body displacement v_0, as suggested by Omar and Hassan (1991, Hassan, 1997), thus obtaining

$$\frac{1}{2(1+\rho^2)}\left(\frac{A_0}{1+\lambda} - 1\right)\theta + \sum_{n=1}^{\infty} A_n f_n \left(\frac{1}{n} - n\right) \ \sin n\theta = 0, \qquad \text{for } 0 \le |\theta| \le \alpha. \qquad (3.13)$$

Then, the procedure used in (Sneddon, 1966; Block and Keer, 2007; Radi and Strozzi, 2023) for solving a similar set of dual series equations is applied to Eqs. (3.6) and (3.13). To this aim, Eq. (3.13) is written in the form

$$\sum_{n=1}^{\infty} A_n \ \sin \ n\theta = (c\, A_0 + d)\theta + \sum_{n=1}^{\infty} h_n\, A_n \ \sin n\theta, \qquad \text{for} \quad 0 \le |\theta| \le \alpha, \qquad (3.14)$$

where

$$\begin{aligned}
&c = \frac{\chi}{2(1+\rho^2)(1+\lambda)},\\
&d = -\frac{\chi}{2(1+\rho^2)}, \qquad (3.15)\\
&h_n = 1 + \chi f_n\left(\frac{1}{n} - n\right),
\end{aligned}$$

where

$$\chi = \begin{cases} 1 & \text{if} \ \ \lambda > 0 \\ 1 - \rho^4 & \text{if} \ \ \lambda = 0 \end{cases} \qquad (3.16)$$

and thus $h_n = O(n^{-1})$ as $n \to \infty$. This asymptotic behavior is necessary for the convergence of the series in Eq. (3.13).

The set of dual equations (3.6) and (3.14) can be solved for the unknown coefficients A_n, for $n = 0, 1, 2, \ldots$, by using the procedure presented by Sneddon (1966) and used by Noble and Hussain (1969), Block and Keer (2007), and Radi and Strozzi (2023), which yields the following system of infinite linear equations:

UNCORRECTED PROOF

$$A_0 = -4(c\,A_0 + d)\ \ln\left(\cos\frac{\alpha}{2}\right) + \sum_{n=1}^{\infty} n\ h_n\, A_n\, J_n, \tag{3.17}$$

$$A_n = (c\,A_0 + d)\, J_n + \frac{1}{2}\sum_{j=1}^{\infty} j\ K_{nj}\ h_j\, A_j, \qquad \text{for} \quad n = 1, 2, \ldots \tag{3.18}$$

where:

$$J_n = \frac{1}{n}\left[P_{n-1}(\cos\alpha) - P_n(\cos\alpha)\right], \tag{3.19}$$

$$K_{nj} = \frac{(1+\cos\alpha)\ \sin^2\alpha}{2(n^2 - j^2)}\left[(n+1)\ P_{j-1}^{(0,1)}(\cos\alpha)\ P_{n-2}^{(1,2)}(\cos\alpha) - (j+1)\ P_{n-1}^{(0,1)}(\cos\alpha)\ P_{j-2}^{(1,2)}(\cos\alpha)\right], \tag{3.20}$$

and $P_n^{(a,b)}(t)$ denotes the Jacobi polynomial of order n. Note that the coefficient K_{nn} in (3.20) is undetermined, but it can be calculated as a limit for $n \to j$. By truncating the sums at a sufficiently large number of terms N, an approximated solution of the linear system of infinite algebraic equations (3.17) and (3.18) for the unknown coefficients A_n can be obtained.

The resultant of the contact pressure distribution $p(\theta)$ along the contact arc must be equal to the total load P applied to the pin, namely

$$P = 2R\int_0^{\alpha} p(\theta)\ \ \cos\theta\ d\theta. \tag{3.21}$$

By using Eqs. (2.4) and (3.6), Eq. (3.21) yields

$$P = -4\mu\delta\int_0^{\alpha}\left(A_0 + 2\sum_{n=1}^{\infty} A_n\ \ \cos n\theta\right)\cos\theta\ d\theta. \tag{3.22}$$

By calculating the definite integral in (2.30), the load P becomes

$$P = -4\mu\delta\ \left[A_0\ \sin\alpha + A_1\left(\alpha + \frac{\sin 2\alpha}{2}\right) + 2\sum_{n=2}^{\infty} A_n \frac{n\ \cos\alpha\ \ \sin n\alpha - \sin\alpha\ \ \cos n\alpha}{n^2 - 1}\right]. \tag{3.23}$$

The rigid body motion of the pin follows from Eq. (3.7) for $\theta = 0$ as

$$\frac{v_0}{\delta} = -\frac{A_0}{1+\lambda} - \frac{A_1}{2(1+\lambda)} - 2(1+\rho^2)\sum_{n=2}^{\infty} A_n f_n. \tag{3.24}$$

4. Results and discussion

The results presented below are obtained for an infinite elastic medium with Poisson's ratio $\nu = 0.3$, under plane-strain conditions. To ensure sufficient accuracy of the semi-analytical solution, at least $N \geq 60$ terms are retained in the truncated system of Eq. (3.17)–(3.18).

The normalized relationship between the pin load P and the pin displacement v_0 is reported in Fig. 2a for several values of the normalized surface elastic modulus λ. Although the advancing contact problem is intrinsically nonlinear, due to the progressive enlargement of the contact region as the pin load increases, the pin load-displacement response becomes nearly linear at sufficiently large loads. Increasing λ markedly enhances the overall contact stiffness, as evidenced by the larger slope of the curves in Fig. 2a.

The normalized variation of the contact half-angle α as a function of the pin-load P is reported in Fig. 2b for the same values of λ considered in Fig. 2a. As the pin load P increases, or equivalently as the radial clearance δ decreases, the contact region expands nonlinearly. Unlike the predictions of classical elasticity, the contact half-angle may exceed $\pi/2$ because of the stiffening effect induced by the surface elastic layer surrounding the hole. In particular, under increasing load, the surface-stiffened ring surrounding the hole tends to elongate in the loading direction while simultaneously contracting in the transverse direction, owing to both the contact pressure along the contact region and the tensile tractions transmitted across the interface between the thin surface layer and the elastic bulk at the free portion of the hole. This mechanism produces an effective constriction of the hole around the rigid pin, thereby promoting the extension of the contact region to angular spans larger than π. Such a behavior becomes increasingly pronounced for large values of λ and represents a distinctive feature of surface elasticity that is absent in classical pin-hole contact models.

The stress and displacement fields along the hole boundary, corresponding to the pin load levels $P = 10\ \mu\delta$ and $P = 20\ \mu\delta$, are analyzed below for different values of the normalized surface elastic modulus λ. For each loading condition, the corresponding contact half-angle α is first determined from the results plotted in Fig. 2. Then, the elastic fields around the hole are evaluated according to the procedure described in Section 2, starting from the calculated values of the contact half-angle α. To mitigate the oscillatory behavior associated with the Gibbs phe-

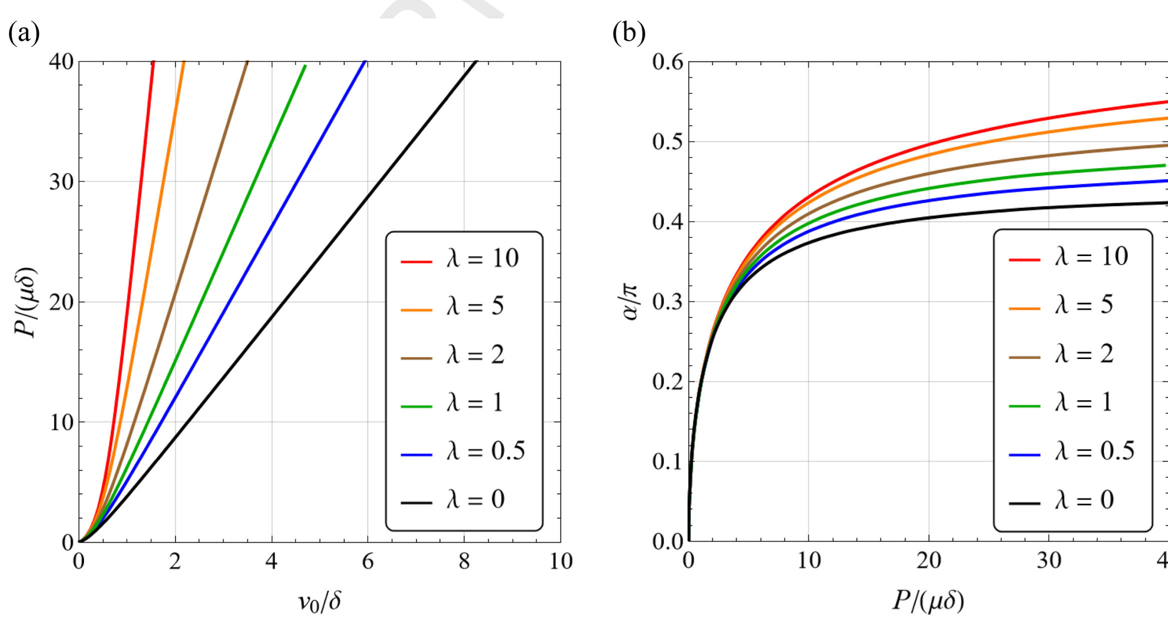

Fig. 2. Normalized variations of the pin load P with the pin displacement v_0 (a), and of the contact half-angle α with the pin load P (b), for some values of the normalized surface elastic modulus λ. For sufficiently large pin load, an almost linear relation is observed between pin load P and pin displacement v_0 (a), and an angular extent of the contact region larger than π is also observed for large values of λ.

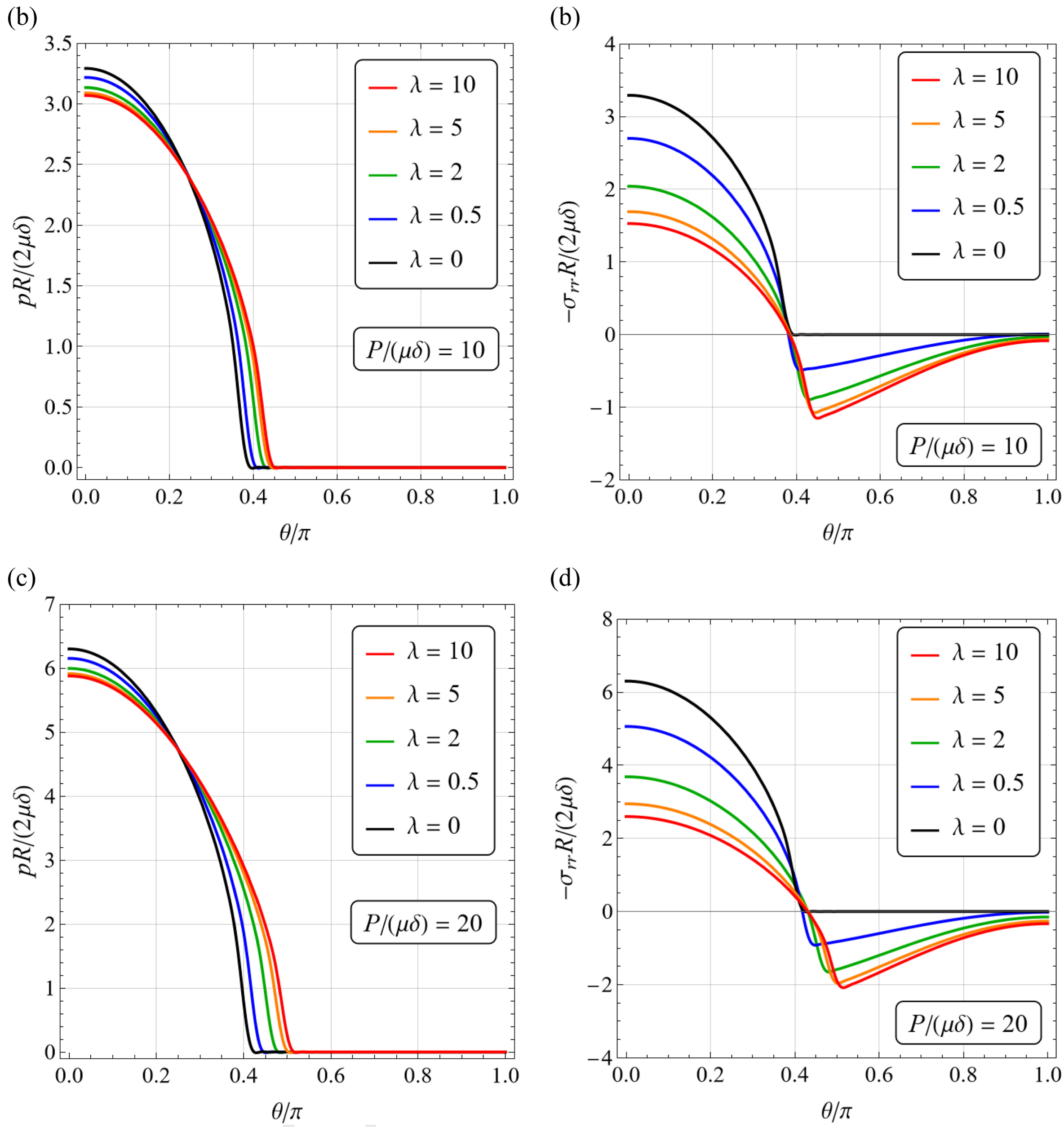

Fig. 3. Normalized distributions of the contact pressure p along the rim of the hole (a, c) and radial stress $-\sigma_{rr}$ along the interface between the thin surface layer and the elastic bulk material (b, d) as functions of the angular coordinate θ. Results are shown for the pin load $P = 10\,\mu\delta$ (a, b) and $P = 20\,\mu\delta$ (c, d), for some values of the normalized surface elastic modulus λ. As λ increases, the size of the contact region slightly increases and the maximum contact pressure decreases correspondingly (a, c). Moreover, the compressive normal stress on the elastic bulk material under the contact region significantly decreases, due to the contribution of the tensile tractions arising between the thin surface layer and the elastic bulk material for $\theta > \pi/2$ (b, d).

nomenon, Lanczos sigma factors (Lanczos, 1956) are introduced into the trigonometric series representation (2.1) of the stress and displacement fields.

The role of surface elasticity is investigated by varying the normalized surface elastic modulus λ. As λ tends to 0, the present formulation consistently recovers the classical solutions for the pin–hole contact problem without surface elasticity (Noble and Hussain, 1969; Mizushima and Hamada, 1983; Omar and Hassan, 1991; Ho and Chau, 1997; Hou and Hills, 2001).

The normalized contact pressure distributions p along the contact surface between the rigid pin and the hole surface are presented in Fig. 3a–c for $P = 10\,\mu\delta$ and $P = 20\,\mu\delta$, respectively, and for some values of the normalized surface elastic modulus λ. The contact pressure profile retains an almost Hertzian character, vanishing smoothly at the contact edges and reaching its maximum at the center of the contact region ($\theta = 0$). In particular, when the surface elastic parameter λ is set to zero the contact pressure distribution of classical elasticity is recovered (Hou and Hills, 2001). However, as λ increases, the contact region slightly enlarges while the maximum contact pressure decreases correspondingly (Fig. 3a–c). This redistribution of the contact pressure indicates that surface elasticity promotes a more diffuse transfer of the load along the contact region. Furthermore, Fig. 3b–d shows a significant reduction in the compressive normal stress transmitted to the elastic bulk beneath the contact region. This effect is directly associated with the tensile load developing in the thin surface layer and with the contribution of the tensile tractions generated along the interface between the surface layer and the substrate in the region $\theta > \pi/2$ (see Fig. 3b–d). Consequently, the load applied to the pin is sustained not only by the compressive stress arising in the

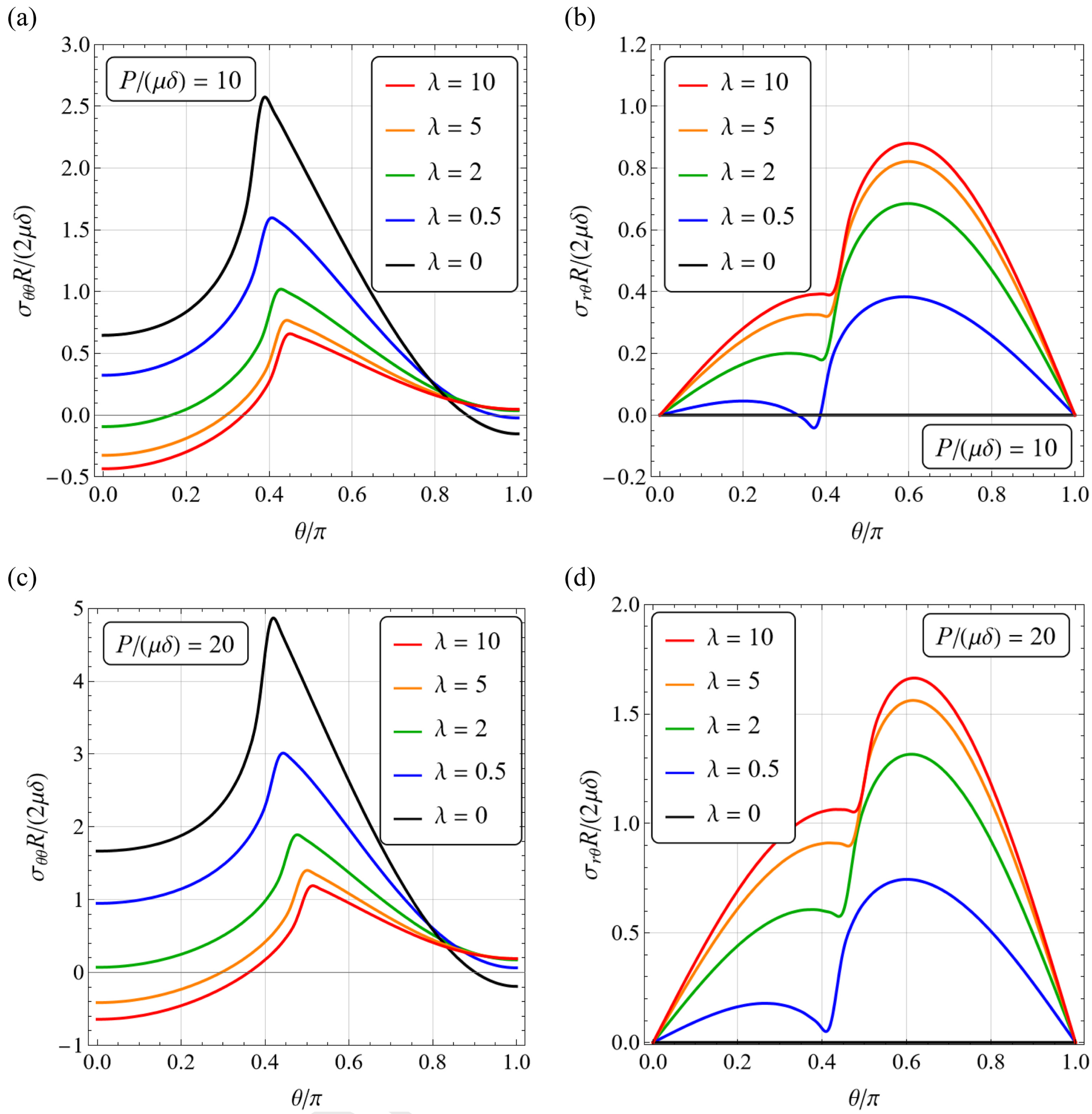

Fig. 4. Normalized distributions of the hoop stress $\sigma_{\theta\theta}$ (a, c) and shear stress $\sigma_{r\theta}$ along the interface between the thin surface layer and the elastic bulk material (b, d) as functions of the angular coordinate θ. Results are shown for the pin load $P = 10\ \mu\delta$ (a, b) and $P = 20\ \mu\delta$ (c, d), for some values of the normalized surface elastic modulus λ. As λ increases, the peak of the hoop stress remarkably increases (a, c), while the maximum shear stress increases correspondingly (b, d).

bulk material beneath the contact region, but also by the tensile and shear stresses distributed throughout the bulk material surrounding the hole surface.

The normalized distributions of the hoop stress $\sigma_{\theta\theta}$ and shear stress $\sigma_{r\theta}$ along the interface between the thin surface layer and the elastic bulk material are plotted in Fig. 4 for $P = 10\ \mu\delta$ (Fig. 4a,b) and $P = 20\ \mu\delta$ (Fig. 4c and d). Increasing the surface elastic modulus substantially reduces the peak hoop stress, leading to a smoother hoop stress distribution along the hole boundary (Fig. 4a–c). For sufficiently large values of λ, the hoop stress at the center of the contact region even becomes compressive, in agreement with the results obtained by Chau and Wei (2001) for a loaded circular inclusion perfectly bonded to an elastic plane through a reinforced ring. Conversely, the maximum shear stress increases with λ, specially along the free portion of the hole boundary, thus denoting a stronger transfer of tangential interaction forces between the surface layer and the substrate (Fig. 4b–d).

The normalized tensile load τ introduced in Eq. (2.3) and developing within the surface layer along the hole boundary is shown in Fig. 5a and b for the two considered loading levels. These results display that the tensile force sustained by the surface layer clearly increases with λ, especially within the contact region, and it is responsible of the transmission of the load to the unloaded region of the hole rim. They also confirm that the surface layer progressively assumes a larger fraction of the transmitted load as its elastic stiffness increases. Therefore, complementary effects of surface elasticity are observed on the bulk hoop stress and on the stress carried by the surface layer. In particular, while surface elasticity may mitigate the hoop stress concentration in the bulk material, it may simultaneously increase the tensile stress sustained by the surface layer.

The normalized radial displacement u_r and tangential displacement u_θ along the hole rim are illustrated in Fig. 6. Results are shown in Fig. 6a and b for $P = 10\ \mu\delta$ and in Fig. 6c and d for $P = 20\ \mu\delta$. As the normalized surface elastic modulus λ increases, the overall magnitude of the displacement field decreases, thus proving the stiffening effect induced by surface elasticity. Indeed, the surface layer acts like an additional circumferential stiffener, in agreement with the findings of Altenbach et al.

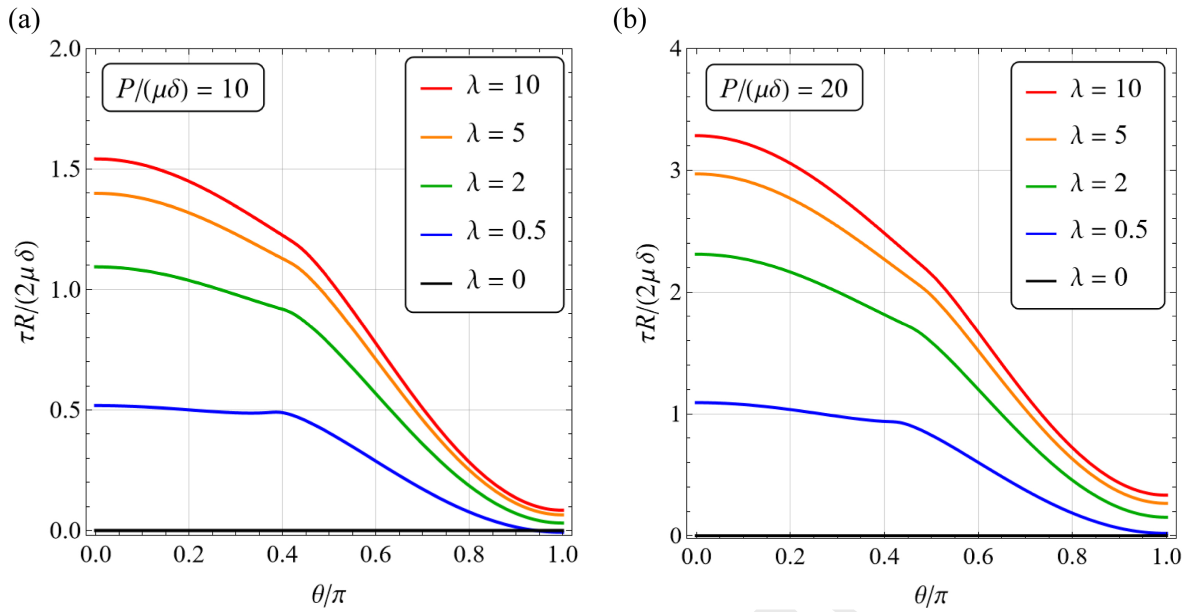

Fig. 5. Normalized distributions of the tensile load τ in the thin surface layer along the hole rim as functions of the angular coordinate θ, under the pin load $P = 10\ \mu\delta$ (a) and $P = 20\ \mu\delta$ (b), for some values of the normalized surface elastic modulus λ. As λ increases, the tensile load τ remarkably increases under the contact region.

(2011). It can be also observed that the radial displacement near $\theta \approx \pi/2$ is negative, with its magnitude increasing as λ increases. This behavior confirms the previously discussed shrinkage of the hole around the rigid pin induced by the surface elastic layer, which is directly associated with the expansion of the contact region beyond π.

To assess the capability of surface elasticity to reduce and redistribute stress concentrations, the contour plots of the von Mises equivalent stress σ_{eq} in the bulk material surrounding the hole are shown in Fig. 7 for three different values of λ, under the same pin load $P = 10\ \mu\delta$, where

$$\sigma_{eq} = \sqrt{\left(1-\bar{\nu}+\bar{\nu}^2\right)(\sigma_{rr}+\sigma_{\theta\theta})^2 - 3\,\sigma_{rr}\sigma_{\theta\theta} + 3\,\sigma_{r\theta}^2}. \tag{4.1}$$

The maximum equivalent stress is consistently attained at the center of the contact region ($\theta = 0$). Its magnitude decreases with increasing the normalized surface elastic modulus λ, in agreement with the general trend of stress-attenuation effect induced by surface elasticity, and remains lower than that predicted by the classical solution corresponding to $\lambda = 0$. At the same time, the equivalent stress along the unloaded portion of the hole boundary increases and gradually approaches the level reached beneath the contact region. This behavior clearly highlights the shielding effect induced by surface elasticity, which alleviates stress concentration in the underlying bulk material.

5. Result consistency check by using the *M*-integral

In a homogeneous linear elastic material, the *M*-integral is a path-independent energy-quantity associated with scaling (dilatation) transformations of the coordinate system. For a circular contour of radius $r > R$ enclosing the hole, the *M*-integral is given by:

$$M = r^2 \int_{-\pi}^{\pi} \left(w - \sigma_{rr}u_{r,r} - \sigma_{r\theta}u_{\theta,r}\right) d\theta, \tag{5.1}$$

where w denotes the strain energy density, which is defined by

$$w = \frac{1}{2}\left(\sigma_{rr}\varepsilon_{rr} + \sigma_{\theta\theta}\varepsilon_{\theta\theta} + 2\sigma_{r\theta}\varepsilon_{r\theta}\right)$$

$$= \frac{1}{2}\left[\sigma_{rr}u_{r,r} + \frac{1}{r}\sigma_{\theta\theta}\left(u_{\theta,\theta}+u_r\right) + \sigma_{r\theta}\left(\frac{u_{r,\theta}-u_\theta}{r} + u_{\theta,r}\right)\right], \tag{5.2}$$

for a linear elastic and isotropic material under plane strain or plane stress loading conditions.

The corresponding *M*-integral (5.1) evaluated along a circle of radius $r > R$, then writes

$$M = r \int_0^{\pi} \left[\sigma_{\theta\theta}\left(u_{\theta,\theta}+u_r\right) - r\sigma_{rr}\, u_{r,r} + \sigma_{r\theta}\left(u_{r,\theta} - u_\theta - r u_{\theta,r}\right)\right] d\theta. \tag{5.3}$$

From a mechanical standpoint, the *M*-integral evaluated over a contour enclosing a cavity can be interpreted as the energetic cost associated with an infinitesimal uniform expansion of the hole (Li and Chen, 2008; Hui and Chen, 2010; Yi-Feng and Chen, 2011;(Hou et al., 2022)).

A particularly useful feature of the *M*-integral is its role as a global invariant that can be exploited for verification purposes. Because of its path independence, it provides a robust consistency check for analytical or numerical solutions. Specifically, when the integral is evaluated along different contours encircling the same region, the result should remain unchanged if the displacement and stress fields satisfy equilibrium, compatibility, and constitutive relations. In this sense, the *M*-integral serves as an energy-based conservation measure for the solution field. In the present work, this invariance property is used as an additional check on the internal consistency of the solution and on the satisfaction of the governing balance laws. In particular, Fig. 8a and b shows the variations of the *M*-integral with the radius r of a circular contour enclosing the pin-loaded hole for various values of the normalized surface elastic modulus λ, and for $P = 10\ \mu\delta$, under plane strain conditions. These results prove that the *M*-integral remains independent of the contour radius for $r > R$, thereby confirming the consistency of the derived stress and displacement fields in the surrounding elastic medium. In addition, the *M*-integral is found to take negative values, with its absolute magnitude increasing as the pin-load P increases. The sign of the *M*-integral reflects the balance between the strain energy stored in the body and the work done by external actions. In particular, a negative value indicates that an infinitesimal increase in the hole radius would lead to an increase in the total potential energy of the system, since $M = -\partial\Pi/\partial R$. While a uniformly pressurized cavity typically yields a positive *M*-integral, a negative response may arise when the additional strain energy accumulated in the surrounding material exceeds the mechanical work performed by the boundary tractions. In the present configuration, the contact pressure along the hole boundary performs positive work during an outward expansion of the hole, which tends to reduce the total potential energy.

UNCORRECTED PROOF

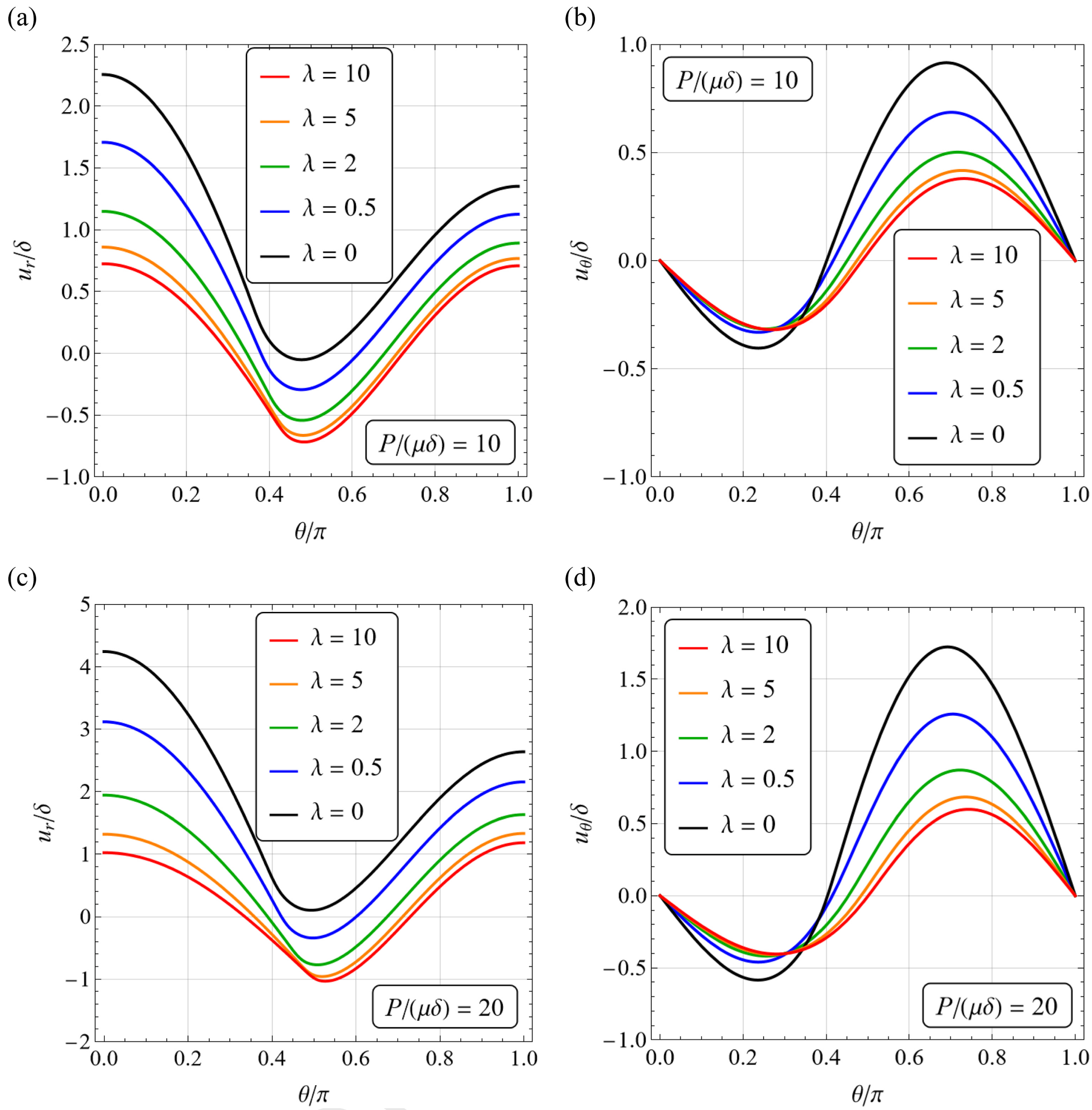

Fig. 6. Normalized distributions of the radial displacement u_r (a, c) and tangential displacement u_θ (b, d) along the hole rim, as functions of the angular coordinate θ. Results are shown for the pin load $P = 10\ \mu\delta$ (a, b) and $P = 20\ \mu\delta$ (c, d), for some values of the normalized surface elastic modulus λ. As λ increases, the magnitude of the displacement field decreases, due to the stiffening effect caused by surface elasticity.

However, this effect is counterbalanced, and ultimately dominated, by the increase in strain energy stored in the elastic medium. When this latter contribution prevails, the M-integral becomes negative, indicating a mechanically resistant configuration with respect to radial expansion. Finally, Fig. 8a and b highlight that λ has a limited and negligible effect on the M-integral. In general, increasing λ yields a more negative M-integral, because surface elasticity makes hole expansion energetically less favourable. This trend can be clearly observed in Fig. 8b for $P = 20\ \mu\delta$, whereas for $P = 10\ \mu\delta$ in Fig. 8a the M-integral assumes very close values for different λ within the range 0-10.

6. Conclusions

An analytical solution has been developed for the contact problem of a rigid circular pin inserted into a hole with a small radial clearance in an infinite elastic medium endowed with surface elasticity along the hole boundary. The governing mixed boundary-value problem has been formulated using Michell-type series expansions for the displacement and stress fields, which allow its transformation into a dual trigonometric series system. This, in turn, is reduced to an infinite system of linear algebraic equations and solved numerically through truncation. The analysis is carried out under both plane strain and plane stress assumptions, although the results are presented with reference to plane strain conditions. The invariance property of the M-integral provides an additional consistency check for the results.

The proposed framework makes it possible to systematically assess the role of surface elasticity in governing the mechanical response of pinned connections. The results indicate that the problem is inherently nonlinear due to the progressive evolution of the contact region with increasing load. In particular, the contact half-angle grows nonlinearly with the applied load and, for sufficiently large values of the normalized surface elastic modulus λ, may extend beyond $\pi/2$. Such behavior, which is not captured by classical elasticity, is a direct consequence of the stiffening and contraction effects induced by the surface layer surrounding the hole.

The contact pressure distribution preserves an essentially Hertz-like

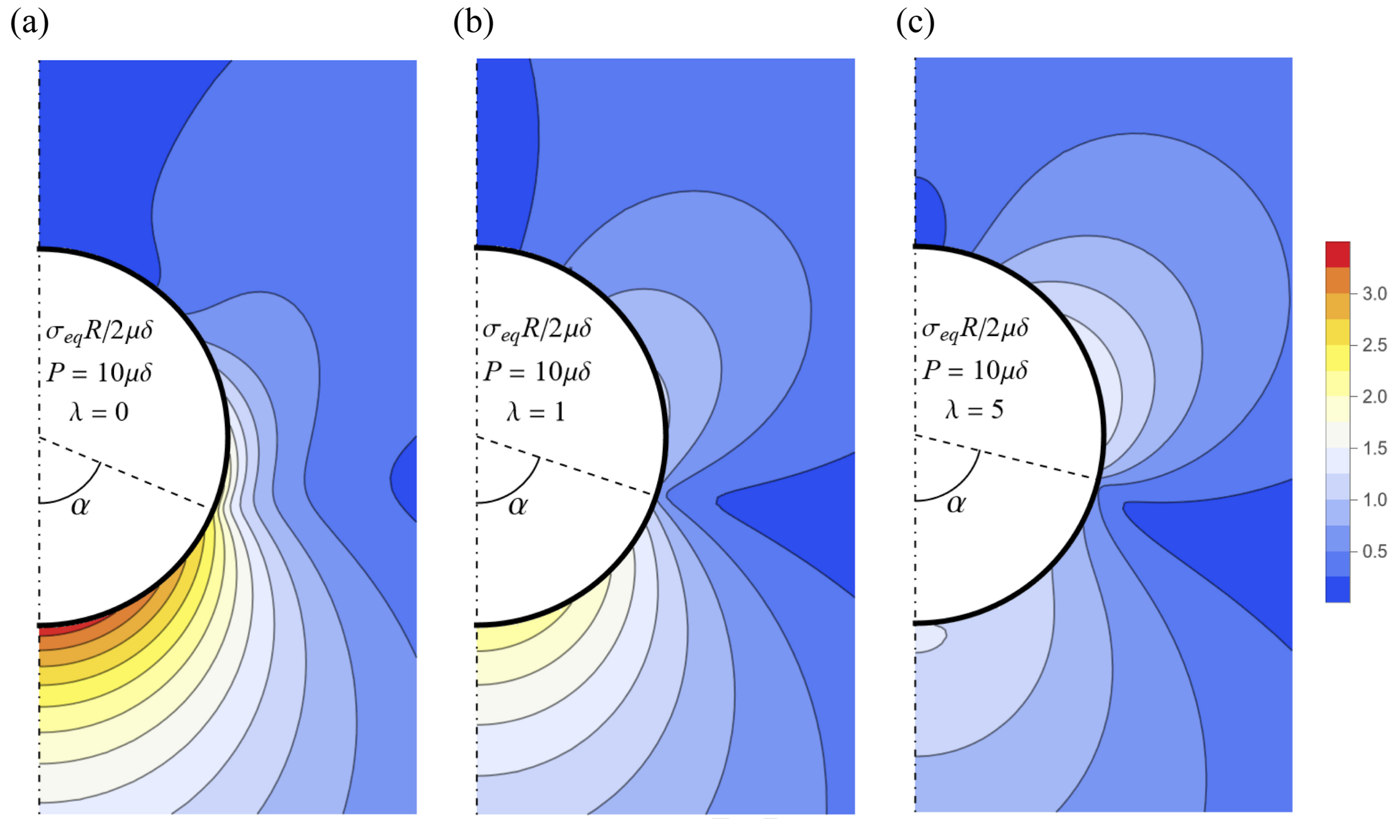

Fig. 7. Analytical distributions of the normalized von Mises equivalent stress $\sigma_{eq}\ R/(2\mu\delta)$ near the hole in the elastic plane under the pin load $P = 20\ \mu\delta$. Results are shown for normalized surface elastic modulus $\lambda = 0$ (a), $\lambda = 1$ (b), and $\lambda = 5$ (c). When surface elastic effects are taken into account, the maximum effective stress within the bulk material is lower than that predicted by the classical solution corresponding to $\lambda = 0$. At the same time, the tractions along the hole boundary become more uniformly distributed, indicating a smoother transfer of the contact load.

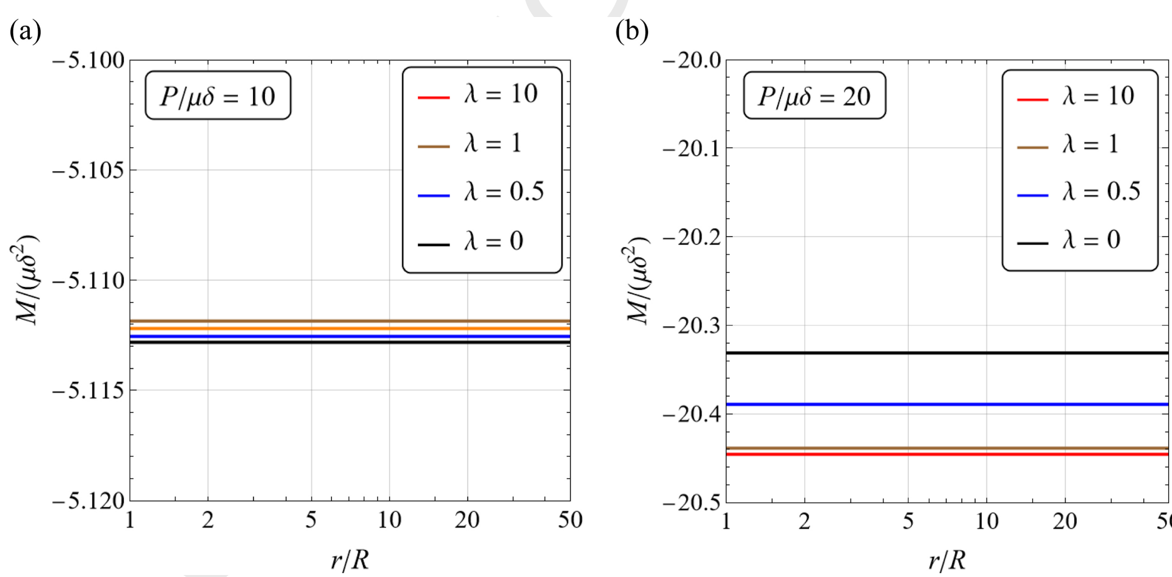

Fig. 8. Normalized variations of the M-integral with the radius r of the closed circular contour enclosing the pin-loaded hole for different values of the normalized surface elastic modulus λ, under the pin load $P = 10\ \mu\delta$ (a) and $P = 20\ \mu\delta$ (b). These results show that the M-integral remains independent of the contour radius for $r > R$, thereby confirming the consistency of the derived stress and displacement fields in the surrounding elastic medium.

character across all loading levels, with a smooth decay to zero at the contact edges and a maximum at the center of the contact zone. Nevertheless, increasing surface elasticity significantly modifies the load transfer mechanism by enlarging the contact region, redistributing contact tractions over a wider portion of the boundary, and reducing the magnitude of both displacement and stress fields. This leads to an overall stiffening of the joint response. Accordingly, peak values of hoop stress and von Mises equivalent stress in the bulk are consistently lower than those predicted by classical elasticity (recovered for $\lambda = 0$), revealing pronounced stress shielding effects associated with the presence of surface elasticity.

The analysis further shows that the surface layer is increasingly engaged in carrying tensile loads as its stiffness increases, while the overall deformation of the joint is progressively suppressed. In particular, the radial displacements in the lateral portions of the hole exhibit a compressive (squeezing) behavior that contributes to the enlargement of the contact region. This mechanism highlights the strong coupling between surface-induced tractions and the global redistribution of contact stresses. In particular, the surface elastic terms introduce tangential derivatives of the displacement into the surface equilibrium equations. These terms penalize rapid variations along the surface and therefore have a smoothing or regularizing effect on the displacement and stress fields, consistently with the general behavior expected in Gurtin-Murdoch surface elasticity.

From an engineering perspective, the results suggest that surface engineering strategies may be effectively employed to control stress concentrations and enhance the mechanical efficiency of pinned joints. The present formulation is therefore relevant to a wide range of applications, including mechanical fastening systems, bearing interfaces, and aerospace joints, where local stress intensification is a critical design limitation. In addition, the model provides useful insights for biomechanical systems, where stiff surface layers overlay compliant substrates, as in cortical–trabecular bone structures. In this context, the present configuration may serve as a simplified representation of biomechanical joints, such as those occurring in hip joint articulation.

Overall, the study demonstrates that surface elasticity provides a powerful mechanism for tailoring contact behavior in pinned connections, offering a viable route toward improved stress management and enhanced structural performance in both engineering and biological systems.

However, it should be emphasized that the present solution corresponds to an infinite-plane idealization with a specific far-field load-transfer mechanism. In finite structural components, the actual remote boundary conditions may alter both the circumferential stress along the hole boundary and the contact pressure distribution. Therefore, for design applications, the present solution should be supplemented by an appropriate open-hole or finite-boundary correction that reflects the actual load path. In particular, the problem of a circular hole located near the free surface of an elastic half-plane and loaded by a rigid pin is currently being investigated using bipolar coordinates. In that configuration, the applied load is transmitted mainly through one side of the body, and different distributions of both hoop stress and contact pressure along the hole boundary are expected.

Declaration of competing interest

The authors declare that they have no known competing financial interests or personal relationships that could have appeared to influence the work reported in this paper.

Acknowledgments

Support by the National Group of Mathematical Physics (GNFM-INdAM) is gratefully acknowledged.

Data availability

No data was used for the research described in the article.

References

Altenbach, H., Eremeyev, V.A., Lebedev, L.P., 2011. On the spectrum and stiffness of an elastic body with surface stresses. Z. Angew. Math. Mech. 91 (9), 699–710.
Barber, J.R., 2010. Elasticity. 3rd Revised Ed. Springer International Publishing, New York.
Block, J.M., Keer, L.M., 2007. Partial contact of an elastic coated cylinder pressed by a rigid flat surface. J. Tribol. 129 (1), 60–64.
Chau, K.T., Wei, X.X., 2001. Stress concentration reduction at a reinforced hole loaded by a bonded circular inclusion. J. Appl. Mech. 68 (3), 405–411.
Ciavarella, M., Decuzzi, P., 2001a. The state of stress induced by the plane frictionless cylindrical contact. I. The case of elastic similarity. Int. J. Solid Struct. 38 (26–27), 4507–4523.
Ciavarella, M., Decuzzi, P., 2001b. The state of stress induced by the plane frictionless cylindrical contact. II. The general case (elastic dissimilarity). Int. J. Solid Struct. 38 (26–27), 4525–4533.
Gerberich, W.W., Tymiak, N.I., Grunlan, J.C., Horstemeyer, M.F., Baskes, M.I., 2002. Interpretations of indentation size effects. J. Appl. Mech. 69 (4), 433–442.
Gurtin, M.E., Murdoch, A.I., 1975. A continuum theory of elastic material surfaces. Arch. Ration. Mech. Anal. 57, 291–323.
Gurtin, M.E., Murdoch, A.I., 1978. Surface stress in solids. Int. J. Solid Struct. 14 (6), 431–440.
Hassan, H.A.Z., 1997. Concentrated force acting on an elastic inclusion in a thick-walled tube. J. Eng. Math. 32, 73–86.
Ho, K.C., Chau, K.T., 1997. An infinite plane loaded by a rivet of a different material. Int. J. Solid Struct. 34 (19), 2477–2496.
Horstemeyer, M.F., Baskes, M.I., 1999. Atomistic finite deformation simulations: a discussion on length scale effects in relation to mechanical stresses. J. Eng. Mater. Technol. 121 (2), 114–119.
Hou, J., Lv, J., Ricoeur, A., Hu, Y., Zuo, H., Chen, Y., Li, Q., 2022. The M-integral in fracture and damage mechanics: a review of developments and applications. Eng. Fract. Mech. 273, 108741.
Hou, J.P., Hills, D.A., 2001. Contact between a pin and a plane with a hole under interference-fit and clearance-fit conditions. Proc. Inst. Mech. Eng. Part C: J. Mech. Eng. Sci. 215 (6), 629–639.
Hui, T., Chen, Y.H., 2010. The M-integral analysis for a nano-inclusion in plane elastic materials under uni-axial or bi-axial loadings. J. Appl. Mech. 77, 21019, 1-9.
Iyer, K., 2001. Solutions for contact in pinned connections. Int. J. Solid Struct. 38 (50–51), 9133–9148.
Lanczos, C., 1956. Applied Analysis. Prentice Hall, Englewood Cliffs.
Li, Q., Chen, Y.H., 2008. Surface effect and size dependence on the energy release due to a nanosized hole expansion in plane elastic materials. J. Appl. Mech. 75 (6), 061008.
Li, X., Mi, C., 2019. Effects of surface tension and Steigmann-Ogden surface elasticity on Hertzian contact properties. Int. J. Eng. Sci. 145, 103165.
Liu, C.S., Zhang, K., Yang, R., 2007. The FEM analysis and approximate model for cylindrical joints with clearances. Mech. Mach. Theor. 42 (2), 183–197.
Long, J.M., Wang, G.F., Feng, X.Q., Yu, S.W., 2012. Two-dimensional Hertzian contact problem with surface tension. Int. J. Solid Struct. 49 (13), 1588–1594.
Mencik, J., 2013. Mechanics of Components with Treated or Coated Surfaces, vol. 42. Springer Science & Business Media.
Mizushima, I., Hamada, M., 1983. Stress analysis around circular hole in infinite plate with rigid disk. Bull. JSME 26 (218), 1296–1301.
Mogilevskaya, S.G., Kushch, V.I., Zemlyanova, A.Y., 2019. Displacements representations for the problems with spherical and circular material surfaces. Quart. J. Mech. Appl. Math. 72 (4), 449–471.
Nguyen, V.L., Nguyen, V.T., Duc, N.D., 2025. Pin-loaded hole contact in an anisotropic magnetoelectro-elastic plate. Int. J. Mech. Sci. 302, 110551.
Nguyen, T.K.H., Nguyen, C.M., 2025. Semi-analytical method for pin-loaded joint contact in anisotropic piezoelectric plates. Int. J. Mech. Sci. 288, 110001.
Nguyen-Hoang, M., Becker, W., 2021. Stress analysis of finite dimensions bolted joints using the Airy stress function. Int. J. Solid Struct. 224, 111023.
Noble, B., Hussain, M.A., 1969. Exact solution of certain dual series for indentation and inclusion problems. Int. J. Eng. Sci. 7 (11), 1149–1161.
Omar, T., Hassan, H.A., 1991. Approximate solution for an indentation problem using dual series equations. Int. J. Eng. Sci. 29 (2), 187–194.
Osborn, H.B., 1941. Surface hardening by induction. Trans. Electrochem. Soc. 79 (1), 215.
Persson, A., 1964. On the Stress Distribution of Cylindrical Elastic Bodies in Contact. Chalmers University, Sweden. PhD. Dissertation.
Persson, E., Eriksson, I., Hammersberg, P., 1997. Propagation of hole machining defects in pin-loaded composite laminates. J. Compos. Mater. 31 (4), 383–408.
Radi, E., Güler, M.A., 2026a. Effects of microstructure in pin-loaded hole contact with clearance. Int. J. Eng. Sci. 221, 104454.
Radi, E., Güler, M.A., 2026b. Pin–hole contact with curvature-induced couple tractions in couple-stress elasticity. Int. J. Solid Struct., 114121.
Radi, E., Strozzi, A., 2023. Advancing contact of a 2D elastic curved beam indented by a rigid pin with clearance. Int. J. Non Lin. Mech. 149, 104313.
Rao, A.K., 1978. Elastic analysis of pin joints. Compos. Struct. 9, 125–144.
Rao, A.K., Eshwar, V.A., Dattaguru, B.A., 1977. Comprehensive study of interference and clearance fit pins in large planes. Mech. Res. Commun. 4 (5), 325–332.
Sneddon, I.N., 1966. Mixed Boundary Value Problems in Potential Theory. John Wiley, New York.
Wang, G.F., Feng, X.Q., 2007. Effects of surface stresses on contact problems at nanoscale. J. Appl. Phys. 101 (1), 013510.
Yavari, V., Daneshvar, F., Kadivar, M.H., Rajabi, I., 2008. Design parameters effect on load distribution around the hole in mechanically fastened pinned connections. In: ASME Pressure Vessels and Piping Conference, 48258, pp. 203–208.
Yi-Feng, H., Chen, Y.H., 2011. The area contraction and expansion for a nano-void under four different kinds of loading. Arch. Appl. Mech. 81 (9), 1323–1331.
Zemlyanova, A.Y., White, L.M., 2022. Axisymmetric frictionless indentation of a rigid stamp into a semi-space with a surface energetic boundary. Math. Mech. Solid 27 (2), 334–347.
Zhou, S., Gao, X.L., 2013. Solutions of half-space and half-plane contact problems based on surface elasticity. Z. Angew. Math. Phys. 64, 145–166.

UNCORRECTED PROOF